RESEARCH ARTICLE

Check for updates

Combination of dimensional reduction and active site addition strategies for preparing unique {RE9}-cluster-based MOFs: efficient CO_2 fixation and Knoevenagel condensation†

Ying Zhao,‡[a] Dan Wu,‡[b,c] Yidan Qiao,[a] Guo-Ping Yang, [ID] *[b] Lu-Fang Ma [ID] *[a,b] and Yao-Yu Wang [ID] [b]

The current application of porous catalytic materials for organic synthesis is always confined to comparatively simple small substrates because of the diffusion barrier. Therefore, in this study, dimensional reduction and active site addition strategies were employed for preparing unique porous {RE9}-cluster-based rare-earth metal–organic frameworks (MOFs) {[Me2NH2]4[RE9(pddb)6(μ3-O)2(μ3-OH)12(H2O)1.5(HCO2)3]·6.5DMF·11H2O}n (**MOF-RE**, RE = Tb, Y, and Dy) with high-density multiple active sites. It was found that **MOF-RE** are rare {RE9}-based two-dimensional (2D) networks including triangular-nanoporous (1.3 nm) and triangular-microporous (0.8 nm) channels decorated by abundant Lewis acid–base sites (open RE(III) sites and $N_{pyridine}$ atoms) on the inner surface. As anticipated, due to the coexistence of Lewis acid–base sites, activated samples exhibited better catalytic activity (a yield of 96%, and a TON value of 768 for styrene oxide) than most previously reported 3D MOF materials for the cyclo-addition of CO_2 and multifarious epoxides under moderate conditions. Moreover, as a heterogeneous catalyst, **MOF-Tb**, has excellent catalytic performance (with a TON value of 396 for benzaldehyde) for the Knoevenagel condensation reaction of malononitrile and aldehydes with high catalytic stability and recoverability. In addition, both reactions possessed high turnover numbers and frequencies. These dimensional reduction and active site addition tactics may permit the exploitation of new nanoporous MOF catalysts based on rare-earth clusters for useful and intricate organic conversions.

Introduction

One of the most important concerns facing all nations on Earth is global climate change, as the main greenhouse gas, carbon dioxide (CO_2) has contributed various severe ecological issues, such as sea level rise and climate change, raising concerns for CO_2 capture and utilization technology.[1–4] The current efficient methods of using CO_2 to create valuable complexes may not only significantly reduce the amount of CO_2 in the environment but also help humanity economically, making them one of the most advantageous options.[5–7] Since cyclic carbonates are a type of extensively utilized chemical and chemical raw material, it has been discovered that producing cyclic carbonates synthetically from epoxides and CO_2 is among the most effective ways to solve environmental issues and realize resource utilization.[8–10] Nevertheless, CO_2 conversion typically involves synergistic catalysis with numerous active sites. Numerous efforts have been made to date to study promising heterogeneous catalysts. Although some are regarded as advantageous, including zeolites,[11] activated carbon,[12] metal oxides[13] and organic polymers,[14] they typically call for high catalytic loadings and harsh conditions, resulting in relatively low yields and conversions with poor recyclability due to the scarcity of catalytic sites.

Metal–organic frameworks (MOFs) containing different polynuclear metal-oxo clusters are unique porous crystalline materials with widespread promise for sensing, heterogeneous catalysis and gas storage/separation.[15–21] Recent studies have exhibited that polynuclear cluster-based rare-earth (RE) MOFs possess exceedingly high stability and abundant catalytic active sites,[22–24] in which the catalytic efficiency for CO_2 con-

[a]*College of Chemistry and Chemical Engineering, Henan Key Laboratory of Function-Oriented Porous Materials, Luoyang Normal University, Luoyang 471934, P.R. China. E-mail: mazhuxp@126.com*
[b]*College of Chemistry and Materials Science, Northwest University, Xi'an 710127, P. R. China. E-mail: ygp@nwu.edu.cn*
[c]*Shaanxi Applied Physics and Chemistry Research Institute, Xi'an 710061, P.R. China*

This journal is © the Partner Organisations 2024

Inorg. Chem. Front., 2024, **11**, 2071–2080 | **2071**

version and Knoevenagel condensation could be greatly accelerated by the synergistic effect of activated metal ions (Lewis acid sites, LASs) and nucleophilic groups (Lewis base sites, LBSs).[25,26] However, the accessibility of these RE-MOF materials to sterically demanding substrates is limited by expanding and stabilizing the active sites. Since the substrates cannot easily reach internal LASs, RE-MOFs perform poorly with larger substrates or complex reactions.[27,28] It is essential to design functional ligands and precisely build RE-microporous MOFs with a high specific surface area and access to multiple active sites *via* an *in situ* function-oriented synthesis strategy to extract the catalytic ability of polynuclear cluster-based RE-MOFs to the greatest extent.

In light of the previous discussion on the standard of functional RE-MOFs as heterogeneous catalysts, this work thoroughly studied the effect of the topological structures of RE-MOFs on the catalytic activity and revealed dimensional reduction and active site addition methods to enhance catalytic reactivity through permitting unrestricted access to Lewis acid–base sites in two-dimensional (2D) MOFs (Scheme 1).[29–31] These strategies can accurately predict the structures of MOFs, so as to achieve the regulation of the catalytic performance.

Hence, a series of unique porous 2D RE-MOFs $\{[Me_2NH_2]_4[RE_9(pddb)_6(\mu_3\text{-}O)_2(\mu_3\text{-}OH)_{12}(H_2O)_{1.5}(HCO_2)_3]\cdot6.5DMF\cdot11H_2O\}_n$ (**MOF-RE**; RE = Tb, Y and Dy) with $\{RE_9\}$ clusters as secondary building units (SBUs) are successfully prepared from C_2-symmetry V-shaped 2,6-bis(4′-carboxyl-phenyl)pyridine (H$_2$pddb) under solvothermal conditions. Notably, **MOF-RE** have high densities of quantified open metal sites (OMSs) acting as LASs and uncoordinated pyridines as LBSs, all of which are exposed in open channels. Benefiting from these active sites, **MOF-RE** exhibits excellent catalytic efficiencies for CO_2 transformation with high yields, turnover numbers (TONs), and turnover frequencies (TOFs) compared to those of many reported 3D MOF materials. Moreover, they have excellent catalytic properties for Knoevenagel condensations *via* the synergistic effects of the LASs and LBSs.

Results and discussion

Description of the crystal structure

The reaction of rare-earth salts (RE = Tb, Dy, and Y) with H$_2$pddb in a mixed solution (DMF/H$_2$O) in the presence of HNO$_3$ and 2-fluorobenzoic acid (2-FBA) gave hexagonal crystals
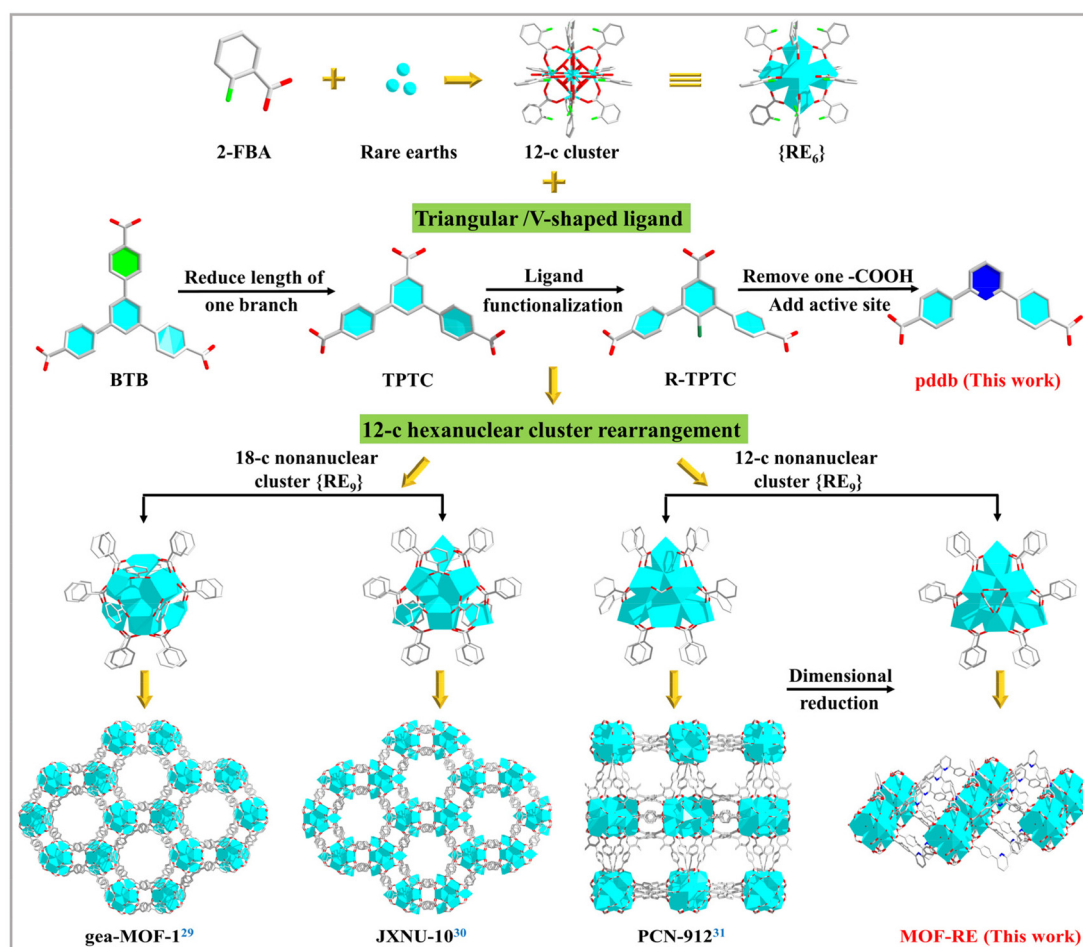
Scheme 1 Different polynuclear cluster-based rare-earth MOFs formed by the $\{RE_9\}$ clusters and functional connectors.

2072 | *Inorg. Chem. Front.*, 2024, **11**, 2071–2080

This journal is © the Partner Organisations 2024

Table 1 Crystal data and structure refinements for **MOF-RE**

Complex	MOF-Tb	MOF-Y	MOF-Dy
Empirical formula	$C_{117}H_{69}N_6O_{45.5}Tb_9$	$C_{117}H_{69}N_6O_{45.5}Y_9$	$C_{117}H_{69}N_6O_{45.5}Dy_9$
Formula mass	3717.06	3086.97	3749.28
Crystal system	Hexagonal	Hexagonal	Hexagonal
Space group	$P6_3/mmc$	$P6_3/mmc$	$P6_3/mmc$
a [Å]	22.5962(4)	22.5233(11)	22.6331(9)
b [Å]	22.5962(4)	22.5233(11)	22.6331(9)
c [Å]	22.7452(5)	22.7551(15)	22.6392(11)
α [°]	90	90	90
β [°]	90	90	90
γ [°]	120	120	120
V [Å^3]	10 057.5(4)	9997.1(12)	10 043.4(9)
Z	2	2	2
$D_{calcd.}$ [g cm^{-3}]	1.227	1.026	1.240
μ [mm^{-1}]	3.173	2.634	3.357
F [000]	3524	3056	3542
θ [°]	2.071–25.349	2.072–25.385	2.078–25.380
Reflections collected	34 562/3409	64 794/3391	66 446/3411
GOOF	1.050	1.061	1.041
$R^{a,b}$ indices [$I > 2\sigma(I)$]	$R_1 = 0.0261$	$R_1 = 0.0419$	$R_1 = 0.0270$
	$wR_2 = 0.0648$	$wR_2 = 0.1209$	$wR_2 = 0.0730$
R indices (all data)	$R_1 = 0.0331$	$R_1 = 0.0590$	$R_1 = 0.0336$
	$wR_2 = 0.0680$	$wR_2 = 0.1303$	$wR_2 = 0.0766$

$^a R_1 = \sum ||F_o| - |F_c||/\sum |F_o|$. $^b wR_2 = [\sum w(F_o{}^2 - F_c{}^2)^2/\sum w(F_o{}^2)^2]^{1/2}$.

of **MOF-RE**. The presence of 2-FBA as a structure guiding agent is an essential condition for the assembly of the polynuclear cluster-based MOFs. The **MOF-RE** crystallize in a primitive hexagonal $P6_3/mmc$ space group (Table 1) and are 2D porous networks. Remarkably, they possess unique polynuclear rare-earth-carboxylate clusters, *i.e.*, a 12-c nonanuclear $[RE_9(\mu_3\text{-}O)_2(\mu_3\text{-}OH)_{12}(O_2C\text{-})_{12}(H_2O)_{1.5}(HCO_2)_3]$ core, in which formates are produced by the breakdown of DMF molecules.[32]

The $[RE_9(\mu_3\text{-}O)_2(\mu_3\text{-}OH)_{12}(O_2C\text{-})_{12}(H_2O)_{1.5}(HCO_2)_3]$ cluster has a threefold symmetry and is composed of nine RE ions arrayed in a {RE$_9$} tricapped trigonal prism, according to detailed research of the nonanuclear cluster (Fig. S1a†). In contrast to the triangular planes of the tetragonal pyramids of the RE$_9$ tricapped trigonal prism, which are each capped by a μ_3-OH, the two triangular planes of the central RE$_6$ trigonal prism are each capped by a μ_3-O (Fig. S1b†). The six RE1 ions are each coordinated with eight O atoms: two from carboxylate moieties of two separate pddb^{2-} connecters and four from four μ_3-OH, and another two coordination sites are composed of O atoms from one HCO$_2{}^-$ ligand and a μ_3-O (O1) (Fig. S2a†). The remaining three RE2 cations are each coordinated with nine O atoms: a terminal H$_2$O molecule, four μ_3-OH and four carboxylate O from four independent pddb^{2-} ligands (Fig. S2a†). The nonanuclear $[RE_9(\mu_3\text{-}O)_2(\mu_3\text{-}OH)_{12}]$ cluster is created by twelve μ_3-OH and two μ_3-O connecting nine RE elements (Fig. 1a) and is terminated through twelve carboxylates from twelve independent pddb^{2-} linkers to generate a 12-connected $[RE_9(\mu_3\text{-}O)_2(\mu_3\text{-}OH)_{12}(O_2C\text{-})_{12}]$ SBU. As the extension point of the $[RE_9(\mu_3\text{-}O)_2(\mu_3\text{-}OH)_{12}(O_2C\text{-})_{12}]$ core, C atoms from the carboxylate groups of twelve independent pddb^{2-} linkers are arranged into a hexagonal prism, which conforms to the d6R vertex diagram of a 12-connected node. There are three H$_2$O molecules and three extra HCO$_2{}^-$ bridging linkers

coordinated with the RE ions to form a nonanuclear $[RE_9(\mu_3\text{-}O)_2(\mu_3\text{-}OH)_{12}(O_2C\text{-})_{12}(H_2O)_{1.5}(HCO_2)_3]$ cluster (Fig. 1a).

In the structure of **MOF-RE**, the pddb^{2-} ligands adopt a bidentate bridging mode to connect two adjacent nonanuclear clusters (Fig. S2b†) to form 2D anionic layers with triangular-microporous (~0.8 nm) and triangular-nanoporous (~1.3 nm) channels (Fig. 1b–d). The 2D infinite layers are stacked along the c axis with an average interlayer spacing of 11.37 Å (Fig. 1e and i). Notably, there are honeycomb-like hexagonal channels with a diameter of ~1.3 nm along the c axis, which are full of protonated $[Me_2NH_2]^+$ cations (Fig. 1f). The porosity computed by PLATON is ~56.1% of the overall crystal volume after excluding free solvents. Topologically, the $[RE_9(\mu_3\text{-}O)_2(\mu_3\text{-}OH)_{12}(O_2C\text{-})_{12}(H_2O)_{1.5}(HCO_2)_3]$ clusters and ligands may act as 12-connected nodes and linear rods, respectively, and the whole structure can be represented as a 12-connected skeleton (Fig. 1g and h).

Gas adsorption studies

MOF-Tb was chosen as a representative for thorough studies due to its isomorphism. The freshly synthesized sample was vacuum-dried at 200 °C for 4 h prior to the sorption test to obtain the activated sample, **MOF-Tba**. The thermogravimetric analysis (TGA) curve was used to explore the activation temperature (Fig. S5†). Simultaneously, the framework integrality of activated **MOF-Tba** was verified *via* the powder X-ray diffraction (PXRD) pattern (Fig. S3†). A 77 K N$_2$ adsorption experiment was performed to confirm the pore properties of **MOF-Tba** (Fig. 2a), indicating that it possesses a traditional type-I adsorption isotherm as well as high Langmuir (825.33 m^2 g^{-1}) and Brunauer–Emmett–Teller (BET) surface areas (560.35 m^2 g^{-1}). The pore size distribution acquired through fitting the 77 K N$_2$-sorption isotherm using nonlocal density functional

This journal is © the Partner Organisations 2024

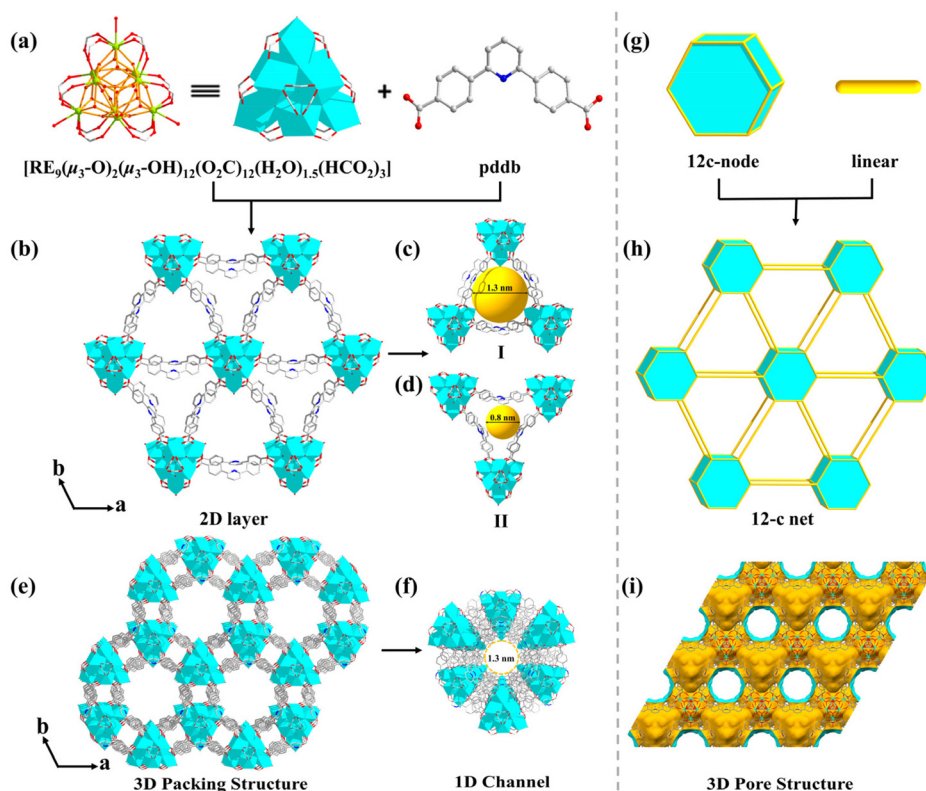*Inorg. Chem. Front.*, 2024, **11**, 2071–2080 | **2073**

Fig. 1 (a and g) Types of {RE$_9$} cluster and ligand and their simplifications; (b and h) 2D structure and corresponding 12-connected net of **MOF-RE**; (c and d) different channels along the *c* axis; (e and f) 3D supramolecular arrangement with 1D hexagonal channels; (i) view of the porous structure of **MOF-RE**.
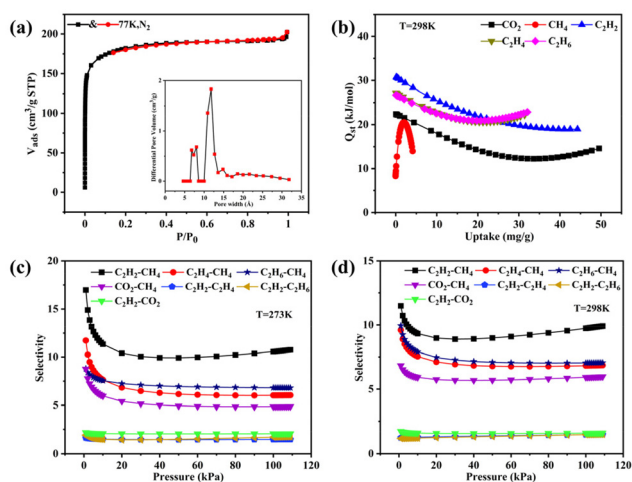

Fig. 2 (a) N$_2$ sorption isotherm at 77 K (inset displays the pore size distribution); (b) gas (C$_2$H$_n$, CO$_2$ and CH$_4$) adsorption heat Q_{st} for **MOF-Tba**. Adsorption selectivities of **MOF-Tba** at 273 K (c) and 298 K (d) calculated using IAST for equimolar mixtures of C$_2$H$_n$/CH$_4$, CO$_2$/CH$_4$, C$_2$H$_2$/C$_2$H$_n$ and C$_2$H$_2$/CO$_2$.

theory is consistent with the pore diameter provided by X-ray crystal data (Fig. 2a).

The latent application of **MOF-Tba** for CO$_2$ and light hydrocarbon (CH$_4$ and C$_2$H$_n$) sorption (Fig. S6 and 7†)/separation

(Fig. 2c and d) has been carefully examined because of its inherent perpetual porosity and channel circumstances. The results displayed that the loading capacity of C$_2$H$_2$ in **MOF-Tba** is higher than that of other gases, demonstrating the maximum interaction between C$_2$H$_2$ and the framework. The sorption enthalpies (Q_{st}) were determined using the virial approach to establish the adsorption affinity between the five gases and skeleton more accurately (Fig. 2b and Fig. S8†). The Q_{st} of **MOF-Tba** to C$_2$H$_2$ (37.6 kJ mol^{-1}) is higher than that of CO$_2$ (22.4 kJ mol^{-1}), C$_2$H$_4$ (27.2 kJ mol^{-1}), C$_2$H$_6$ (26.7 kJ mol^{-1}), and CH$_4$ (8.6 kJ mol^{-1}) under zero coverage, which agrees with the measured adsorption amount. Moreover, the possibility of separating CH$_4$ from light hydrocarbons was studied by ideal solution adsorbed theory (IAST) for binary equimolar mixtures (Fig. S9 and 10†).[33] The selectivities for CO$_2$, C$_2$H$_2$, C$_2$H$_4$ and C$_2$H$_6$ over CH$_4$ at 1 bar and 298 K are 5.9, 9.8, 6.8 and 7.0, respectively (Fig. 2c), making **MOF-Tba** an exceptional sorbent for effectively removing CO$_2$/C$_2$ light hydrocarbons from natural gas.

Catalytic performance for CO$_2$ conversion

Considering that **MOF-Tba** has the advantages of solvent-accessible nanoscale channels, high specific surface area and abundant coexisting Lewis acid–base sites ([Tb$_9$(μ$_3$-O)$_2$(μ$_3$-OH)$_{12}$(O$_2$C)$_{12}$(H$_2$O)$_{1.5}$(HCO$_2$)$_3$] clusters and N$_{pyridine}$ atoms), it

was employed as an effective heterogeneous catalyst for the cyclo-addition of CO_2 and epoxy complexes (Scheme S1†). Our previous study[34] has shown that the catalysts were not recycled and exhibited poor activity due to the lack of high-density active sites when selecting the pddb ligand itself and physical mixture of the rare-earth metal-pddb ligand to catalyze this reaction. Therefore, this study conducted a range of control experiments based on styrene oxide, determined ideal reaction conditions, such as time, temperature, and catalyst dosage and identified products through ^{1}H NMR spectroscopy (Fig. S14–25†).

Entry 1 (Table 2) displays that when **MOF-Tba** (0.05 mol%) was added as a catalyst, only a small amount of product with a yield of 5% was detected within 12 h. In addition, only a slight conversion (10%) could be observed under the cocatalyst of n-Bu$_4$NBr (1 mol%) alone, as shown in entry 2. Nevertheless, the yield was tremendously improved 29% (entry 3) when **MOF-Tba** (0.05 mol%) and n-Bu$_4$NBr (1 mol%) were concurrently introduced to the reaction, suggesting that **MOF-Tba** and n-Bu$_4$NBr synergistically activated the second-order reaction of CO_2 and epoxides. Increasing the temperature was used to demonstrate that one of the key factors was temperature for influencing the reaction outcome, as shown in entries 4 and 5. Furthermore, entries 6 and 7 examined and listed the effect of the cocatalyst n-Bu$_4$NBr dosage, which demonstrated that the quantity of the cocatalyst had a clear impact on the reaction rate. The yield increased to 95% when 5 mol% n-Bu$_4$NBr cocatalyst was added. The amount of **MOF-Tba** was increased because the practical application of the catalyst will be severely hampered by the 12 h reaction time. Styrene oxide could be converted into 4-phenyl-1,3-dioxolan-2-one more rapidly, as described in entries 8–10. In conclusion, it was found that the ideal reaction conditions are 0.125 mol% **MOF-Tba** catalyst, 5 mol% n-Bu$_4$NBr cocatalyst, 60 °C and 6 h. In addition, we performed a detailed analysis of the ^{1}H NMR spectrum for entry 10, confirming that no by-products were generated during the reaction (Fig. S19†).

The catalytic universality of **MOF-Tba** was further evaluated utilizing a range of propylene oxide derivatives with distinct substituents and steric hindrance under determined ideal reaction circumstances (Table 3). The outcomes indicated that there was some regularity in how different substituents affected the yield. It can be seen from the comparison of entries 1 and 2 that the epoxy complexes with electron-withdrawing groups (–Br and –Cl) could improve the efficiency of the cycloaddition reaction, and the yield could reach more than 99%, the reason for which is that the electron-withdrawing group may decrease the electron density of ethylene oxide.[35,36] In contrast, electron-donating groups had a disadvantageous impact on this process, as in entry 3.[37,38] Furthermore, entries 4–6 exhibited a significant decrease in the conversion of epoxide with bulky substituents, confirming the idea that big substituents restrict the mobility of substrate molecules.[39–42] Table S1† lists information about the molecular sizes of all epoxide derivatives. Additionally, the TON of **MOF-Tba** for styrene oxide was notable compared to most reported TON values for MOF catalysts (Table S2†), which was likely attributable to the profitable contribution of {Tb$_9$} clusters and abundant N$_{pyridine}$ groups in the channels.

The actual organic synthesis industry depends heavily on the stability and recyclability of catalysts;[43] hence, additional tests were conducted about hot leaching, recovery, and recycling of **MOF-Tba**. First, the recycling stability of **MOF-Tba** for the cyclization reaction of CO_2 with styrene oxide was studied under the determined ideal reaction conditions. The conversion of styrene oxide was nearly unchanged for five cycles by the recovered catalyst **MOF-Tba** (Fig. S11†). Meanwhile, the PXRD pattern of the recovered **MOF-Tba** sample after five experiments was essentially matched with the newly formed one, showing that the **MOF-Tba** catalyst maintained the stability of the framework (Fig. S12†). Afterward, inductively coupled plasma (ICP) analysis was then used in leaching experiments. As a result, the recovered filtrate included just a little quantity of Tb(III) ions (0.015%), further demonstrating the stability of **MOF-Tba** in the organic reaction. Furthermore, a thermal filtration experiment was carried out, and the results showed that the reaction hardly happens when the catalyst is filtered out (Fig. S13†), meaning that **MOF-Tba** possessed a heterogeneous nature.

The probable catalytic mechanism can be deduced from prior MOF-related literature,[44–47] and the distinctive structural characteristics of **MOF-Tba**, including high specific surface area, functional channel, and plentiful {Tb$_9$} clusters (Fig. 3). First, the epoxide rapidly diffuses into the **MOF-Tba** catalyst and makes weak contact with its exposed metal sites in a confined environment. Then, the nucleophilic attack of less-obstructed carbon atoms in the epoxide by the Br$^-$ anion released by n-Bu$_4$NBr promotes the formation of the alkylcarbonate anion. Subsequently, polarized CO_2 molecules tend to undergo nucleophilic addition reactions with alkylcarbonate anions to generate alkylcarbonate salt. Finally, the ring closure behavior results in the production of cyclic carbonate and liberation of catalysts.

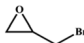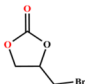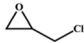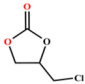## Catalytic performances for Knoevenagel condensation
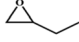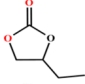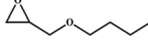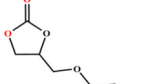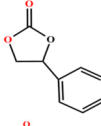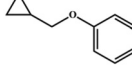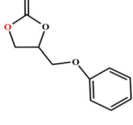
Knoevenagel condensation is a classical C–C bond coupling reaction, and its reaction mechanism involves the covalent

Table 2 Cycloaddition of CO_2 with styrene oxide under different conditions[a]

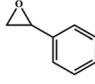| Entry	MOF (mol%)	n-Bu$_4$NBr (mol%)	T (°C)	t (h)	Yield[b] (%)
1	0.05	0	25	12	5
2	0	1	25	12	10
3	0.05	1	25	12	32
4	0.05	1	40	12	54
5	0.05	1	60	12	78
6	0.05	3	60	12	86
7	0.05	5	60	12	95
8	0.075	5	60	10	94
9	0.1	5	60	8	95
10	0.125	5	60	6	96

[a] Reaction conditions: solvent-free, styrene oxide (20 mmol), and CO_2 (1 atm). [b] The product yield was determined by ^{1}H NMR.

Table 3 Cycloaddition of CO_2 with epoxides under optimal conditions[a]

Entry	Epoxide	Product	Yield[b] (%)	TON[c]	TOF[d] (h^{-1})
1			>99	792	132
2			>99	792	132
3			96	768	128
4			96	768	128
5			96	768	128
6			95	760	127

[a] Reaction conditions: solvent-free, epoxides (20 mmol), n-Bu$_4$NBr (5 mol%), Tb-MOF catalyst (0.125 mol%), CO_2 (1 atm), 60 °C, and 6 h. [b] Yield was determined by ^{1}H NMR. [c] TON = [product (mmol)]/[catalyst (mmol)]. [d] TOF = TON/time.
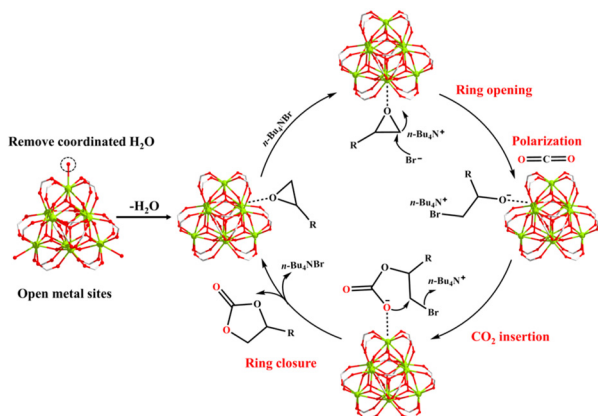
Fig. 3 Proposed mechanism of CO_2 conversion catalyzed by **MOF-Tba**.

C=C bond formed by the carbonyl group combining with the methylene group activated *via* both electron-withdrawing moieties.[40–42,48] Pharmaceuticals and fine compounds are frequently synthesized using this process. Recent research has proven that active metal centers (LASs) and nucleophilic moieties (LBSs) in porous MOFs could work together to significantly speed up the Knoevenagel reaction.[49–52] Therefore, more research was done on active porous **MOF-Tba** to catalyze the Knoevenagel condensation (Scheme S2†).

Initially, perfect reaction conditions were studied with benzaldehyde and malononitrile as substrates in the presence of desolvated **MOF-Tba** as a heterogeneous catalyst, as seen in

Table 4 and Fig. S29–31.† Entry 1 shows that only trace 2-benzylidenemalono-nitrile (3%) was produced at 25 °C without the catalyst **MOF-Tba**, whereas when **MOF-Tba** (0.1 mol%) was introduced, a yield of 38% was generated within 2 h (entry 2), indicating that the reaction could scarcely be carried out without the catalyst. The conversion of the substrate increased progressively when all other factors governing the reaction were held constant, and only the catalyst dosage was increased (entries 3 and 4). At 25 °C, the yield was 85% when the **MOF-Tba** dosage was raised to 0.25 mol% (entry 5). The reaction substrate was virtually entirely converted as the temperature rose from 25 °C to 60 °C in parallel investigations using 0.25 mol% **MOF-Tba** (entries 6 and 7), demonstrating that

Table 4 Knoevenagel condensation from substrates of benzaldehyde and malononitrile[a]

Entry	**MOF-Tba** (mol%)	Time (h)	T (°C)	Yield[b] (%)
1	0	2	25	3
2	0.1	2	25	38
3	0.15	2	25	58
4	0.2	2	25	76
5	0.25	2	25	85
6	0.25	2	40	93
7	0.25	2	60	99
8	0.25	1.5	60	95
9	0.25	1	60	88
10	0.25	0.5	60	65

[a] Reaction conditions: malononitrile (20 mmol), benzaldehyde (10 mmol). [b] The product yield was determined by ^{1}H NMR.

2076 | *Inorg. Chem. Front.*, 2024, **11**, 2071–2080

This journal is © the Partner Organisations 2024

temperature was one of the crucial elements in the condensation reaction. Additionally, the connection between the conversion with reaction time was examined under the reaction environments of 0.25 mol% **MOF-Tba** at 60 °C (entries 8–10). It can be seen from the above results that the ideal reaction conditions were 0.25 mol% **MOF-Tba**, 60 °C, and 2 h when the ratio of malononitrile to aldehyde was 2 : 1.

Based on aforementioned discoveries, we chose several aldehyde derivatives with various substituents and steric hindrance (Table S3†) to confirm the **MOF-Tba** catalyst's suitability for the Knoevenagel condensation reaction, and the outcomes are displayed in Table 5 and Fig. S32–38.†

Entries 2–4 show that the conversion efficiency of benzaldehyde with electron-drawing groups (–F, –Br, and –NO$_2$) surpassed 99%, whereas the catalytic yield was slightly decreased due to the presence of the electron-donating groups (–CH$_3$ and –CH$_2$CH$_3$) (entries 5 and 6), indicating that the electron-donating moieties greatly inhibit the Knoevenagel condensation reaction. Additionally, the conversion efficiency clearly reduced as the molecular size and steric hindrance of the substrate increased (entry 7). Remarkably, benzaldehyde had a TON value of 396, which was much higher than the majority of previously documented MOF catalysts (Table S4†).

The best experimental conditions were used to study the stability and recyclability of **MOF-Tba**. The utilized **MOF-Tba** catalyst was recovered and repeatedly cleaned with DMF after each reaction. Over 97% of 2-benzylidenemalono-nitrile was produced after five repetitions of the process using **MOF-Tba**, which retained excellent catalytic activity (Fig. S26†). Furthermore, the PXRD peaks of gathered **MOF-Tba** demonstrated that the host framework remained unchanged, suggesting the great stability of the microporous hetero-

geneous catalyst (Fig. S27†). Following the catalytic recycling experiment, leached homogenous Tb(III) was monitored by ICP analysis as well. The probability of leaching metal ions from the **MOF-Tba** network during Knoevenagel condensation was ruled out when trace Tb(III) of 0.018% was found in the filtrate. Under optimal reaction circumstances, a heat filtration test was conducted to confirm the heterogeneous nature of **MOF-Tba**. The solid catalyst was filtered out after the reaction had been going on for 0.5 hours. Since the conversion rate barely altered (Fig. S28†), the heterogeneous nature of **MOF-Tba** was further supported.

Fig. 4 implies a likely catalytic reaction mechanism based on relevant published studies[53–59] and structural characteristics of **MOF-Tba**. First, the carbonyl oxygen of the aldehyde
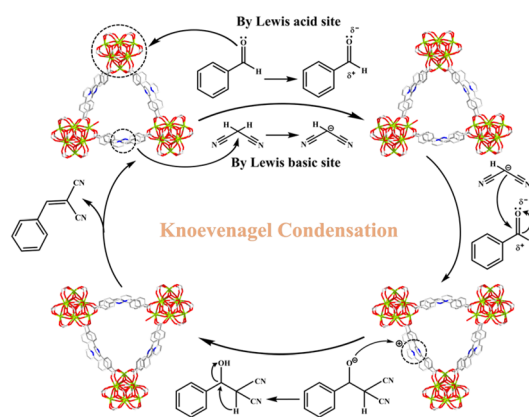

Fig. 4 Proposed mechanism for Knoevenagel condensation by **MOF-Tba**.

Table 5 Knoevenagel condensation reaction of aldehyde derivatives under optimal conditions[a]

Entry	Substrate	Product	Yield[b] (%)	TON[c]	TOF[d] (h^{-1})
1			>99	396	198
2			>99	396	198
3			>99	396	198
4			>99	396	198
5			98	384	192
6			94	372	186
7			87	348	174

[a] Reaction conditions: aldehyde derivatives (10 mmol), malononitrile (20 mmol), catalyst **MOF-Tba** (0.25 mol%), 2 h, 60 °C. [b] The yield was calculated by ^{1}H NMR. [c] TON = [product (mmol)]/[catalyst (mmol)]. [d] TOF = TON/time.

group made a weak interaction with the exposed Tb(III) sites of **MOF-Tba**, converting its carbon atom into a positive carbon center and initiating the reaction. Simultaneously, $N_{pyridine}$ atoms as the LBSs caused the carbonyl carbon of malononitrile to polarize into a negative center. Second, a covalent bond was formed between two carbon atoms with opposing electric charges, resulting in an imine intermediate. Finally, the recombination of intramolecular electrons combined with the release of H_2O molecules and the used catalyst resulted in the formation of the product benzylidenemalononitrile.

Conclusions

A series of 2D {RE$_9$}-cluster-based rare-earth **MOF-RE** with Lewis acid–base dual functional sites were designed and synthesized by dimensional reduction and active site addition strategies. As expected, they benefited from high-density active sites and had exceptional catalytic properties for the chemical fixation of CO_2 with epoxides under moderate conditions, together with satisfactory catalytic efficiencies for Knoevenagel condensation. These strategies proposed in this work not only provide a new method for the preparation of nanoporous cluster-based RE-MOFs with various catalytic activities but also lay a foundation for the research of the catalytic mechanism.

Conflicts of interest

There are no conflicts to declare.

Acknowledgements

References

1   C. Wang, B. An and W. Lin, Metal–Organic Frameworks in Solid–Gas Phase Catalysis, *ACS Catal.*, 2018, **9**, 130–146.

2   J. F. Kurisingal, Y. Rachuri, A. S. Palakkal, R. S. Pillai, Y. Gu, Y. Choe and D. W. Park, Water-Tolerant DUT-Series Metal–Organic Frameworks: A Theoretical–Experimental Study for the Chemical Fixation of CO_2 and Catalytic Transfer Hydrogenation of Ethyl Levulinate to γ-Valerolactone, *ACS Appl. Mater. Interfaces*, 2019, **11**, 41458–41471.

3   J. Liu, G. P. Yang, J. Jin, D. Wu, L. F. Ma and Y. Y. Wang, A first new porous d–p HMOF material with multiple active sites for excellent CO_2 capture and catalysis, *Chem. Commun.*, 2020, **56**, 2395–2398.

4   J. Liu, Y. Z. Fan, X. Li, Y. W. Xu, L. Zhang and C. Y. Su, Catalytic Space Engineering of Porphyrin Metal–Organic Frameworks for Combined CO_2 Capture and Conversion at a Low Concentration, *ChemSusChem*, 2018, **11**, 2340–2347.

5   P. Das and S. K. Mandal, Unprecedented High Temperature CO_2 Selectivity and Effective Chemical Fixation by a Copper-Based Undulated Metal–Organic Framework, *ACS Appl. Mater. Interfaces*, 2020, **12**, 37137–37146.

6   J. Liu, Y. Wei and Y. Zhao, Trace Carbon Dioxide Capture by Metal–Organic Frameworks, *ACS Sustainable Chem. Eng.*, 2018, **7**, 82–93.

7   S. L. Hou, J. Dong, X. L. Jiang, Z. H. Jiao and B. Zhao, A Noble-Metal-Free Metal–Organic Framework (MOF) Catalyst for the Highly Efficient Conversion of CO_2 with Propargylic Alcohols, *Angew. Chem., Int. Ed.*, 2019, **58**, 577–581.

8   E. Liu, J. Zhu, W. Yang, F. Liu, C. Huang and S. Yin, PCN-222(Co) Metal–Organic Framework Nanorods Coated with 2D Metal–Organic Layers for the Catalytic Fixation of CO_2 to Cyclic Carbonates, *ACS Appl. Nano Mater.*, 2020, **3**, 3578–3584.

9   Z. Zhang, J.-H. Ye, T. Ju, L.-L. Liao, H. Huang, Y.-Y. Gui, W.-J. Zhou and D.-G. Yu, Visible-Light-Driven Catalytic Reductive Carboxylation with CO_2, *ACS Catal.*, 2020, **10**, 10871–10885.

10 X. Yang, Q. Zou, T. Zhao, P. Chen, Z. Liu, F. Liu and Q. Lin, Deep Eutectic Solvents as Efficient Catalysts for Fixation of CO_2 to Cyclic Carbonates at Ambient Temperature and Pressure through Synergetic Catalysis, *ACS Sustainable Chem. Eng.*, 2021, **9**, 10437–10443.

11 M. R. Hudson, W. L. Queen, J. A. Mason, D. W. Fickel, R. F. Lobo and C. M. Brown, Unconventional, Highly Selective CO_2 Adsorption in Zeolite SSZ-13, *J. Am. Chem. Soc.*, 2012, **134**, 1970–1973.

12 Y. Zhang, B. Li, K. Williams, W. Y. Gao and S. Ma, A new microporous carbon material synthesized via thermolysis of a porous aromatic framework embedded with an extra carbon source for low-pressure CO_2 uptake, *Chem. Commun.*, 2013, **49**, 10269–10271.

13 P. R. Tambe and G. D. Yadav, Heterogeneous cycloaddition of styrene oxide with carbon dioxide for synthesis of styrene carbonate using reusable lanthanum–zirconium mixed oxide as catalyst, *Clean Technol. Environ. Policy*, 2018, **20**, 345–356.

14 Y. Xie, T. T. Wang, X. H. Liu, K. Zou and W. Q. Deng, Capture and conversion of CO_2 at ambient conditions by a conjugated microporous polymer, *Nat. Commun.*, 2013, **4**, 1960.

15 H. Wang, X. Liu, W. Yang, G. Mao, Z. Meng, Z. Wu and H. L. Jiang, Surface-Clean Au$_{25}$ Nanoclusters in Modulated Microenvironment Enabled by Metal–Organic Frameworks for Enhanced Catalysis, *J. Am. Chem. Soc.*, 2022, **144**, 22008–22017.

16 P. F. Gao, Y. Y. Jiang, H. Liu, M. S. Zhou, T. Li, H. R. Fu, L. F. Ma and D. S. Li, Pillar-Layer Chiral MOFs as a Crystalline Platform for Circularly Polarized Luminescence and Single-Phase White-Light Emission, *ACS Appl. Mater. Interfaces*, 2022, **14**, 16435–16444.

2078 | *Inorg. Chem. Front.*, 2024, **11**, 2071–2080

This journal is © the Partner Organisations 2024

17 R.-Y. Chen, Y.-P. He, G.-H. Chen and J. Zhang, Designing Cage-Supported Cluster-Organic Framework for Highly Efficient Optical Limiting, *ACS Mater. Lett.*, 2022, **4**, 1397–1401.

18 Z. H. Zhu, Z. L. Liang, Z. H. Jiao, X. L. Jiang, Y. Xie, H. Xu and B. Zhao, A Facile Strategy to Obtain Low-Cost and High-Performance Gold-Based Catalysts from Artificial Electronic Waste by $[Zr_{48}Ni_6]$ Nano-Cages in MOFs for CO_2 Electroreduction to CO, *Angew. Chem., Int. Ed.*, 2022, **61**, e202214243.

19 Q. Y. Wang, Z. B. Sun, M. Zhang, S. N. Zhao, P. Luo, C. H. Gong, W. X. Liu and S. Q. Zang, Cooperative Catalysis between Dual Copper Centers in a Metal–Organic Framework for Efficient Detoxification of Chemical Warfare Agent Simulants, *J. Am. Chem. Soc.*, 2022, **144**, 21046–21055.

20 J. L. Li, X. Xiong, D. Luo, Y. B. Wei, W. Lu and D. Li, Formaldehyde recognition through aminal formation in a luminescent metal–organic framework, *Chem. Commun.*, 2022, **58**, 6490–6493.

21 H. Yang, Y. Chen, C. Dang, A. N. Hong, P. Feng and X. Bu, Optimization of Pore-Space-Partitioned Metal–Organic Frameworks Using the Bioisosteric Concept, *J. Am. Chem. Soc.*, 2022, **144**, 20221–20226.

22 S. A. Younis, N. Bhardwaj, S. K. Bhardwaj, K.-H. Kim and A. Deep, Rare earth metal–organic frameworks (RE-MOFs): Synthesis, properties, and biomedical applications, *Coord. Chem. Rev.*, 2021, **429**, 213620.

23 H. A. Bicalho, P. R. Donnarumma, V. Quezada-Novoa, H. M. Titi and A. J. Howarth, Remodelling a shp: Transmetalation in a Rare-Earth Cluster-Based Metal–Organic Framework, *Inorg. Chem.*, 2021, **60**, 11795–11802.

24 H. A. Bicalho, F. Saraci, J. J. Velazquez-Garcia, H. M. Titi and A. J. Howarth, Unravelling the synthesis of a rare-earth cluster-based metal–organic framework with spn topology, *Chem. Commun.*, 2022, **58**, 10925–10928.

25 T. Zhang, H. Chen, S. Liu, H. Lv, X. Zhang and Q. Li, Highly Robust $\{Ln_4\}$-Organic Frameworks (Ln = Ho, Yb) for Excellent Catalytic Performance on Cycloaddition Reaction of Epoxides with CO_2 and Knoevenagel Condensation, *ACS Catal.*, 2021, **11**, 14916–14925.

26 J. Qiao, B. Zhang, L. Zhang and Y. Liu, Practice of function-oriented synthesis: high-efficiency CO_2 conversion and Knoevenagel condensation by two novel In_3-based MOFs with high-density active sites under mild conditions, *J. Mater. Chem. A*, 2022, **10**, 17773–17781.

27 D. Yang and B. C. Gates, Catalysis by Metal Organic Frameworks: Perspective and Suggestions for Future Research, *ACS Catal.*, 2019, **9**, 1779–1798.

28 H. Chen, S. Liu, H. Lv, Q. P. Qin and X. Zhang, Nanoporous $\{Y_2\}$-Organic Frameworks for Excellent Catalytic Performance on the Cycloaddition Reaction of Epoxides with CO_2 and Deacetalization–Knoevenagel Condensation, *ACS Appl. Mater. Interfaces*, 2022, **14**, 18589–18599.

29 V. Guillerm, L. Weselinski, Y. Belmabkhout, A. J. Cairns, V. D'Elia, L. Wojtas, K. Adil and M. Eddaoudi, Discovery and introduction of a (3,18)-connected net as an ideal blueprint for the design of metal–organic frameworks, *Nat. Chem.*, 2014, **6**, 673–680.

30 L. Chen, H. J. Hu, Y. L. Wang, X. F. Zhang, L. P. Xu and Q. Y. Liu, Metal–Organic Frameworks Featuring 18-Connected Nonanuclear Rare-Earth Oxygen Clusters and Cavities for Efficient C_2H_2/CO_2 Separation, *Inorg. Chem.*, 2021, **60**, 13471–13478.

31 Y. Wang, L. Feng, W. Fan, K. Y. Wang, X. Wang, X. Wang, K. Zhang, X. Zhang, F. Dai, D. Sun and H. C. Zhou, Topology Exploration in Highly Connected Rare-Earth Metal–Organic Frameworks via Continuous Hindrance Control, *J. Am. Chem. Soc.*, 2019, **141**, 6967–6975.

32 A. Rossin, G. Giambastiani, M. Peruzzini and R. Sessoli, Amine-Templated Polymeric Lanthanide Formates: Synthesis, Characterization, and Applications in Luminescence and Magnetism, *Inorg. Chem.*, 2012, **51**, 6962–6968.

33 D. Alezi, A. M. Peedikakkal, L. J. Weselinski, V. Guillerm, Y. Belmabkhout, A. J. Cairns, Z. Chen, L. Wojtas and M. Eddaoudi, Quest for Highly Connected Metal–Organic Framework Platforms: Rare-Earth Polynuclear Clusters Versatility Meets Net Topology Needs, *J. Am. Chem. Soc.*, 2015, **137**, 5421–5430.

34 D. Wu, X. Lu, Y. Tang, F. Gao, G. Yang and Y.-Y. Wang, Light-Assisted CO_2 Cycloaddition over a Nanochannel Cadmium–Organic Framework Loaded with Silver Nanoparticles, *ACS Appl. Nano Mater.*, 2023, **6**, 6197–6207.

35 H. Chen, L. Fan and X. Zhang, Highly Robust 3s–3d $\{CaZn\}$–Organic Framework for Excellent Catalytic Performance on Chemical Fixation of CO_2 and Knoevenagel Condensation Reaction, *ACS Appl. Mater. Interfaces*, 2020, **12**, 54884–54892.

36 Y. B. N. Tran, P. T. K. Nguyen, Q. T. Luong and K. D. Nguyen, Series of M-MOF-184 (M = Mg, Co, Ni, Zn, Cu, Fe) Metal–Organic Frameworks for Catalysis Cycloaddition of CO_2, *Inorg. Chem.*, 2020, **59**, 16747–16759.

37 S. Liu, H. Chen and X. Zhang, Bifunctional $\{Pb_{10}K_2\}$–Organic Framework for High Catalytic Activity in Cycloaddition of CO_2 with Epoxides and Knoevenagel Condensation, *ACS Catal.*, 2022, **12**, 10373–10383.

38 Q. R. Ding, Y. Yu, C. Cao, J. Zhang and L. Zhang, Stepwise assembly and reversible structural transformation of ligated titanium coated bismuth-oxo cores: shell morphology engineering for enhanced chemical fixation of CO_2, *Chem. Sci.*, 2022, **13**, 3395–3401.

39 N. Seal and S. Neogi, Intrinsic-Unsaturation-Enriched Biporous and Chemorobust Cu(II) Framework for Efficient Catalytic CO_2 Fixation and Pore-Fitting Actuated Size-Exclusive Hantzsch Condensation with Mechanistic Validation, *ACS Appl. Mater. Interfaces*, 2021, **13**, 55123–55135.

40 G. Jin, D. Sensharma, N. Zhu, S. Vaesen and W. Schmitt, A highly augmented, (12,3)-connected Zr-MOF containing hydrated coordination sites for the catalytic transformation

This journal is © the Partner Organisations 2024

Inorg. Chem. Front., 2024, **11**, 2071–2080 | **2079**

of gaseous CO_2 to cyclic carbonates, *Dalton Trans.*, 2019, **48**, 15487–15492.

41 Y. Li, X. Zhang, J. Lan, D. Li, Z. Wang, P. Xu and J. Sun, A High-Performance Zinc-Organic Framework with Accessible Open Metal Sites Catalyzes CO_2 and Styrene Oxide into Styrene Carbonate under Mild Conditions, *ACS Sustainable Chem. Eng.*, 2021, **9**, 2795–2803.

42 B. Ugale, S. S. Dhankhar and C. M. Nagaraja, Construction of 3-Fold-Interpenetrated Three-Dimensional Metal–Organic Frameworks of Nickel(II) for Highly Efficient Capture and Conversion of Carbon Dioxide, *Inorg. Chem.*, 2016, **55**, 9757–9766.

43 K. Maity, C. K. Karan and K. Biradha, Porous Metal-Organic Polyhedral Framework containing Cuboctahedron Cages as SBUs with High Affinity for H2 and CO_2 Sorption: A Heterogeneous Catalyst for Chemical Fixation of CO_2, *Chem. – Eur. J.*, 2018, **24**, 10988–10993.

44 Z. Xue, J. Jiang, M.-G. Ma, M.-F. Li and T. Mu, Gadolinium-Based Metal–Organic Framework as an Efficient and Heterogeneous Catalyst To Activate Epoxides for Cycloaddition of CO_2 and Alcoholysis, *ACS Sustainable Chem. Eng.*, 2017, **5**, 2623–2631.

45 B. Parmar, P. Patel, R. S. Pillai, R. I. Kureshy, N.-U. H. Khan and E. Suresh, Efficient catalytic conversion of terminal/internal epoxides to cyclic carbonates by porous Co(II) MOF under ambient conditions: structure–property correlation and computational studies, *J. Mater. Chem. A*, 2019, **7**, 2884–2894.

46 A. Shaabani, R. Mohammadian, H. Farhid, M. K. Alavijeh and M. M. Amini, Multitask Guanidinium Bromide Functionalized Metal–Organic Framework in Chemical Fixation of CO_2 at Low Pressure and Temperature, *Ind. Eng. Chem. Res.*, 2019, **58**, 8553.

47 F. Norouzi and H. R. Khavasi, Diversity-Oriented Metal Decoration on UiO-Type Metal–Organic Frameworks: an Efficient Approach to Increase CO_2 Uptake and Catalytic Conversion to Cyclic Carbonates, *ACS Omega*, 2019, **4**, 19037–19045.

48 T. Stolar, A. Prasnikar, V. Martinez, B. Karadeniz, A. Bjelic, G. Mali, T. Friscic, B. Likozar and K. Uzarevic, Scalable Mechanochemical Amorphization of Bimetallic Cu–Zn MOF-74 Catalyst for Selective CO_2 Reduction Reaction to Methanol, *ACS Appl. Mater. Interfaces*, 2021, **13**, 3070–3077.

49 C. I. Ezugwu, B. Mousavi, M. A. Asraf, Z. Luo and F. Verpoort, Post-synthetic modified MOF for Sonogashira cross-coupling and Knoevenagel condensation reactions, *J. Catal.*, 2016, **344**, 445–454.

50 M. Opanasenko, A. Dhakshinamoorthy, M. Shamzhy, P. Nachtigall, M. Horáček, H. Garcia and J. Čejka, Comparison of the catalytic activity of MOFs and zeolites in Knoevenagel condensation, *Catal. Sci. Technol.*, 2013, **3**, 500–507.

51 R. Sharma, A. Bansal, C. N. Ramachandran and P. Mohanty, A multifunctional triazine-based nanoporous polymer as a versatile organocatalyst for CO_2 utilization and C–C bond formation, *Chem. Commun.*, 2019, **55**, 11607–11610.

52 S. Yuan, L. Huang, Z. Huang, D. Sun, J. S. Qin, L. Feng, J. Li, X. Zou, T. Cagin and H. C. Zhou, Continuous Variation of Lattice Dimensions and Pore Sizes in Metal–Organic Frameworks, *J. Am. Chem. Soc.*, 2020, **142**, 4732–4738.

53 Y. Luan, Y. Qi, H. Gao, R. S. Andriamitantsoa, N. Zheng and G. Wang, A general post-synthetic modification approach of amino-tagged metal–organic frameworks to access efficient catalysts for the Knoevenagel condensation reaction, *J. Mater. Chem. A*, 2015, **3**, 17320–17331.

54 F. Ghobakhloo, D. Azarifar, M. Mohammadi, H. Keypour and H. Zeynali, Copper(II) Schiff-Base Complex Modified $UiO-66-NH_2(Zr)$ Metal–Organic Framework Catalysts for Knoevenagel Condensation–Michael Addition–Cyclization Reactions, *Inorg. Chem.*, 2022, **61**, 4825–4841.

55 Q. Xu, B. Xu, H. Kong, P. He, J. Wang, T. Kannan, P. Ma, J. Wang and J. Niu, Synthesis and Characterization of a Crown-Shaped 36-Molybdate Cluster and Application in Catalyzing Knoevenagel Condensation, *Inorg. Chem.*, 2020, **59**, 10665–10672.

56 G. Q. Huang, J. Chen, Y. L. Huang, K. Wu, D. Luo, J. K. Jin, J. Zheng, S. H. Xu and W. Lu, Mixed-Linker Isoreticular Zn(II) Metal–Organic Frameworks as Brønsted Acid–Base Bifunctional Catalysts for Knoevenagel Condensation Reactions, *Inorg. Chem.*, 2022, **61**, 8339–8348.

57 Z.-S. Zhao, Y. Zhang, T. Fang, Z.-B. Han and F.-S. Liang, Chitosan-Coated Metal–Organic-Framework Nanoparticles as Catalysts for Tandem Deacetalization–Knoevenagel Condensation Reactions, *ACS Appl. Nano Mater.*, 2020, **3**, 6316–6320.

58 F. Kalantari, S. Rezayati, A. Ramazani, H. Aghahosseini, K. Ślepokura and T. Lis, Proline-Cu Complex Based 1,3,5-Triazine Coated on Fe_3O_4 Magnetic Nanoparticles: A Nanocatalyst for the Knoevenagel Condensation of Aldehyde with Malononitrile, *ACS Appl. Nano Mater.*, 2022, **5**, 1783–1797.

59 J. Qiao, B. Zhang, X. Yu, X. Zou, X. Liu, L. Zhang and Y. Liu, A Stable Y(III)-Based Amide-Functionalized Metal–Organic Framework for Propane/Methane Separation and Knoevenagel Condensation, *Inorg. Chem.*, 2022, **61**, 3708–3715.

2080 | *Inorg. Chem. Front.*, 2024, **11**, 2071–2080

This journal is © the Partner Organisations 2024